Hindawi
Advances in Condensed Matter Physics
Volume 2022, Article ID 6001569, 7 pages
https://doi.org/10.1155/2022/6001569

Research Article

Structural and Morphological Properties of Single and Mixed Halide Pb-Based Perovskites

Kanij Fatema,[1,2] **Mohammad Tanvir Ahmed**,[1] **Md. Kamal Hossain**,[1] **and Farid Ahmed**[1]

[1]*Department of Physics, Jahangirnagar University, Savar, Dhaka-1342, Bangladesh*
[2]*Department of Electrical and Electronic Engineering, Bangladesh University of Business and Technology (BUBT), Dhaka-1216, Bangladesh*

Correspondence should be addressed to Kanij Fatema; priankajun@gmail.com

Received 5 July 2022; Accepted 27 September 2022; Published 11 October 2022

Academic Editor: Junjie Li

Single and mixed-halide perovskite solar cells have attracted much research attention in recent years due to the conditions of low-cost thin film solar cell technology. For this current research, perovskite materials $CH_3NH_3PbCl_3$, $CH_3NH_3PbI_2Cl$, $CH_3NH_3PbICl_2$, and $CH_3NH_3PbI_3$ have been synthesized and deposited on clean glass substrates by spin coating process. The structural and morphological properties of the prepared thin films have been studied by X-ray diffraction and Scanning electron microscopy. All the perovskite showed fine crystallinity, possessing a tetragonal phase. The average crystallite sizes of the prepared samples are obtained to be 20.77 nm, 30.18 nm, 31.11 nm, and 42.23 nm, respectively. The lattice strain decreased with increasing crystallite size. A drastic change was observed in the morphological properties of the perovskites. The perovskite grains change from microrods to microcube by substituting iodine with chlorine ions.

1. Introduction

Nowadays, organic-inorganic perovskite solar cells (PSCs) based on organometallic halides are an emerging photovoltaic technology. Perovskites are attractive, highly crystalline hybrids because of their unity of organic and inorganic materials [1]. These hybrid perovskites take advantage of combining distinct properties of inorganic and organic components within a single molecular material [2, 3]. Compared with other solar cells, PSCs have low production costs because of their simple synthesis procedure, mainly solution-based process [4, 5], and fabrication without any complexity by using spin coating process [6, 7]. Lead-based perovskites, mainly $CH_3NH_3PbI_3$ ($MAPI_3$), are the most harvested material for PSCs [8, 9]. The $MAPI_3$ material has a better excitation coefficient with excellent external quantum efficiency until 800 nm of wavelength, and this material shows the highest efficiency [10, 11].

The general chemical formula of organometallic perovskite compound is ABX_3, where A and B are organic cation and divalent metal cation, respectively, and X is the halogen anion [12].

PSCs were first reported in 2009, achieving 3.81% power conversion efficiency (PCE). A breakthrough came in 2012, Lee et al. obtained a PCE of 10.9% perovskite mixed-halide $CH_3NH_3PbI_2Cl$ using a "mesoporous device architecture." By 2013, a simple planar heterojunction solar cell combining vapor-deposited perovskite ($MAPbI_{3-x}Cl_x$) as an absorbing layer was reported to have a PCE over 15% [13] which proved that nanostructure is not required to obtain high efficiency. They used a perovskite absorber and mesoporous TiO_2 as *n*-type transporter materials. They replaced mesoporous *n*-type TiO_2 with Al_2O_3, acting as a "scaffold," which improved the efficiency, and the perovskite film was 150 nm thick [14]. Although Pb is a toxic element, Pb-based perovskite shows better performance in various fields compared to other metal-based perovskites [15–24]. Jeong et al. reported high-efficiency PSCs with a PCE of 17% by size-controlled growth of $MAPI_3$ cuboids [17]. Nei et al. synthesized a millimeter-sized grain of $MAPbI_{3-x}Cl_x$ perovskite via the spin coating method resulting in a PCE of 18% [18]. Perovskite-based solar cells' PCE achieved 19.3% using a planar geometry without an

antireflective layer. They used the perovskite absorber $CH_3NH_3PbI_{3-X}Cl_X$ [19]. PCE up to 20.4% was reported in 2016 to achieve reproducible MAPI perovskite solar cells through the grain boundary healing process [20]. According to the NREL chart, the efficiency of Pb-based perovskite solar cells recently reached 25.2% based on single-junction architectures and 29.1% in silicon tandem cells in 2020 [25]. Mo et al. synthesized Zirconia coated Pb-based perovskite nanocrystals for light emitting diode (LED) applications, which showed enhanced stability and better luminescence [16]. Wang et al. a developed $CsPbBr_3$@Polymethyl methacrylate composite which showed improved performance as X-ray scintillators [21]. Zhou et al. studied superalkali introduced perovskites' solar cell performance and obtained up to 22.83% PCE with $H_5O_2PbBr_3$ [23].

A material's optical and electrical properties are heavily influenced by its crystal structure and surface morphology. A material can have varied crystal shapes and phases depending on the crystal development conditions. Doping, heating, concentration variation, and other means can also be used to alter the crystal structure and surface morphology.

Here, Lead-based perovskite materials $CH_3NH_3PbI_3$ ($MAPI_3$), $CH_3NH_3PbI_2Cl$ ($MAPI_2Cl$), $CH_3NH_3PbICl_2$ ($MAPICl_2$), and $CH_3NH_3PbCl_3$ ($MAPCl_3$) were synthesized via one-step spin coating method. In this work, the synthesized materials' basic structural and morphological properties are studied using X-ray diffraction (XRD) and scanning electron microscopy (SEM), respectively.

2. Experimental

2.1. Reagents. CH_3NH_2 (40%), HI (67% in H_2O), HCl (32% in H_2O), lead (II) chloride (99%, Merck), and lead (II) iodide (99%, Sigma–Aldrich).

2.2. Synthesis of the Perovskite Structures. Methylamine (MA, CH_3NH_2) was reacted with Hydroiodic acid (HI) with a molar ratio of 1 : 1 to produce CH_3NH_3I. Similarly, CH_3NH_2 and HCl were reacted with a 1 : 1 molar ratio to synthesize CH_3NH_3Cl [26].

0.01 mole CH_3NH_3Cl and CH_3NH_3I were dissolved separately into 10 mL·N, N-dimethylformamide (DMF). An Equimolar ratio of $PbCl_2$ and PbI_2 dissolved in DMF containing CH_3NH_3Cl and CH_3NH_3I, respectively, to produce $CH_3NH_3PbCl_3$ and $CH_3NH_3PbI_3$ precursor solution [27, 28]. Similarly, an equimolar ratio of $PbCl_2$ and PbI_2 were reacted with CH_3NH_3I and CH_3NH_3Cl, respectively, to synthesize $CH_3NH_3PbICl_2$ and $CH_3NH_3PbI_2Cl$, respectively [29, 30]. Figure 1 shows the prepared perovskite precursor solutions.

The precursor solutions of $CH_3NH_3PbI_3$, $CH_3NH_3ClPbI_2$, $CH_3NH_3IPbCl_2$, and $CH_3NH_3PbCl_3$, were spin coated on glass substrates at 1500 rpm for 30 sec (Figure 2). Then, deposited films were annealed at 60° for 20 minutes.

2.3. Characterizations. The structural properties were obtained by X-ray diffraction analysis via the GBC EMMA diffractometer. Surface morphology was studied by ZEISS Evo18 SEM.

3. Results and Discussion

3.1. Structural Analysis. XRD pattern of $MAPI_3$ (Figure 3) satisfies previous research showing peaks at $2\theta = 14.48°$, 28.72°, 32.19°, and 43.47° which correspond to (100), (200), (210), and (211), respectively [12, 31]. $MAPI_2Cl$ depicts peaks at $2\theta = 11.13°$, 13.14°, 31.72°, 39.03°, 52.55° which correlate to (100), (110), (211), (221), and (400) planes, respectively. (001), (100), and (111) planes of $MAPICl_2$ perovskites are identified at $2\theta = 14.38°$, 28.57°, and 43.54°, respectively [24]. For $MAPCl_3$, peaks are procured at $2\theta = 16.0°$, 32.02°, 48.51° correlating to (002), (103), and (211) planes, respectively [32, 33]. Higher 2θ values correspond to decreasing interplanner spacing and increasing peak width [34, 35].

The lattice parameters of the prepared crystals were calculated via "FullProf" software and listed in Table 1. It is observed that all the synthesized perovskites possess a tetragonal crystal phase with a variation in lattice parameters which is caused by the structural deformation due to the variation of halide ion stoichiometry. The alteration of halide ions can generate residual stress in the lattice due to the variation of X-site ion radius, which can vary the lattice constants as well as the interplanar spacing of the crystals. As a result, the variation of unit cell parameters is observed.

The grain size of synthesized materials has been calculated from the X-ray diffraction pattern using the Debye–Scherrer equation [36].

$$\text{Crystallite size, } L = \frac{K\lambda}{\beta \cos \theta}, \tag{1}$$

where β, λ, and K are full-width half-maxima (FWHM), X-ray wavelength, and Scherrer constant (~0.89), respectively.

The average crystallite sizes of $MAPI_3$, $MAPI_2Cl$, $MAPICl_2$, and $MAPCl_3$ structures are listed in Table 2. The crystallite size is related to the dislocation density (δ) by the following equation:

$$\delta = \frac{1}{L^2}. \tag{2}$$

Which represents the number of dislocations per unit length [12]. Since δ makes an inverse square relation with L, smaller crystallite size possesses higher dislocations. The crystallite size and dislocation density suggest that the periodicity of perovskites increases with decreasing iodine content and increasing chlorine content.

The lattice strain (ε) is a measure of deformation in the crystal structure and can be obtained from the following equation [12],

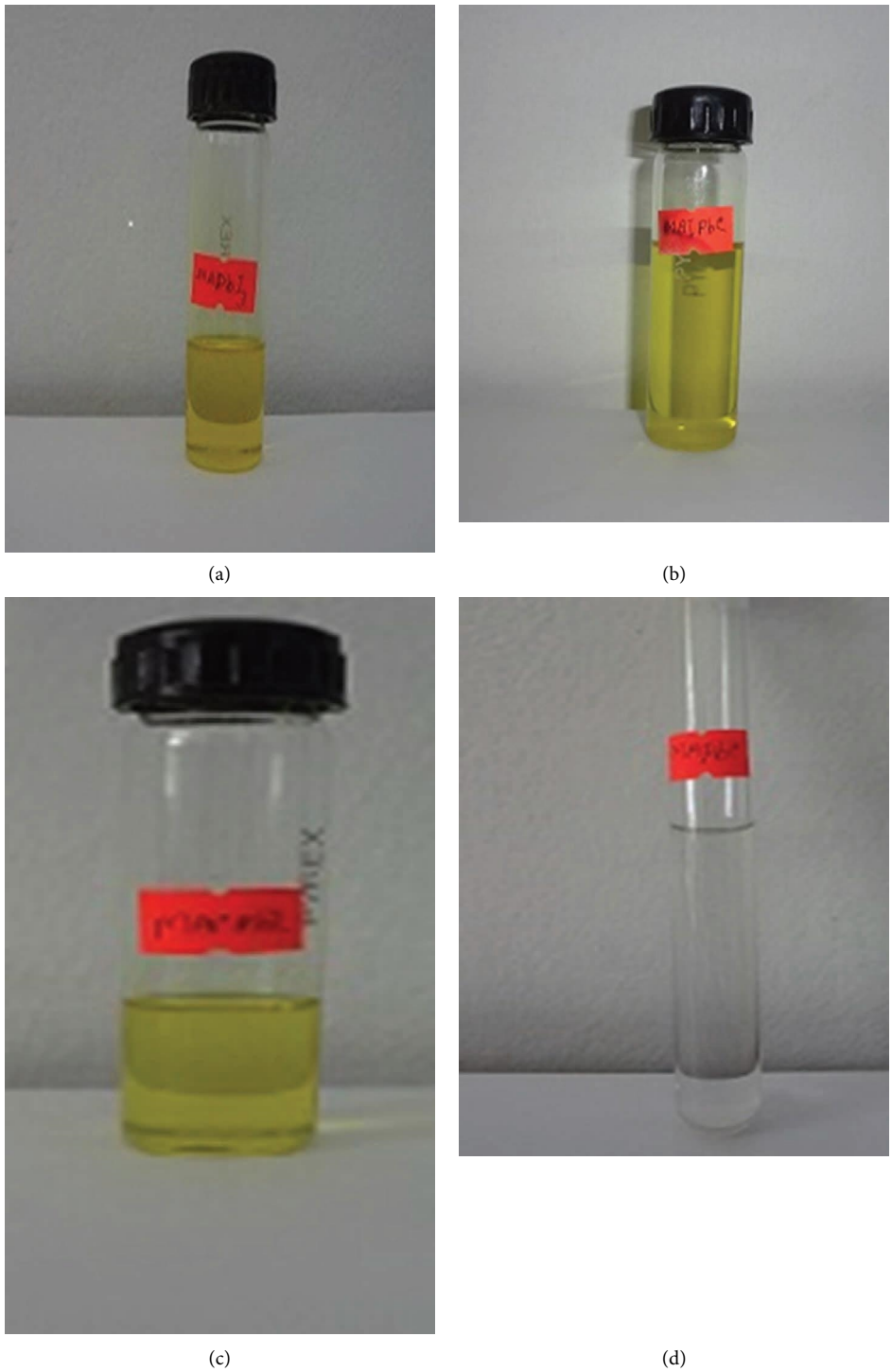

(a) (b) (c) (d)

Figure 1: Synthesized (a) $CH_3NH_3PbI_3$, (b) $CH_3NH_3ClPbI_2$, (c) $CH_3NH_3IPbCl_2$, and (d) $CH_3NH_3PbCl_3$ precursor solutions.

$$\varepsilon = \frac{\beta}{4 \tan \theta}. \tag{3}$$

The strains of $MAPI_3$, $MAPI_2Cl$, $MAPICl_2$, and $MAPCl_3$ are 0.0087, 0.0081, 0.0067, and 0.0043, respectively. The strain decreases with iodine reduction in the perovskite structure (Figure 4). The lattice strain can vary due to the difference in different halide ionic radii and the variation in the thermal expansion coefficient of the substrate and deposited crystals [12, 37]. The reduction of lattice strain represents less deformation in the crystal structure, which can offer higher periodicity. As a result, the crystallite size has increased with decreasing iodine content.

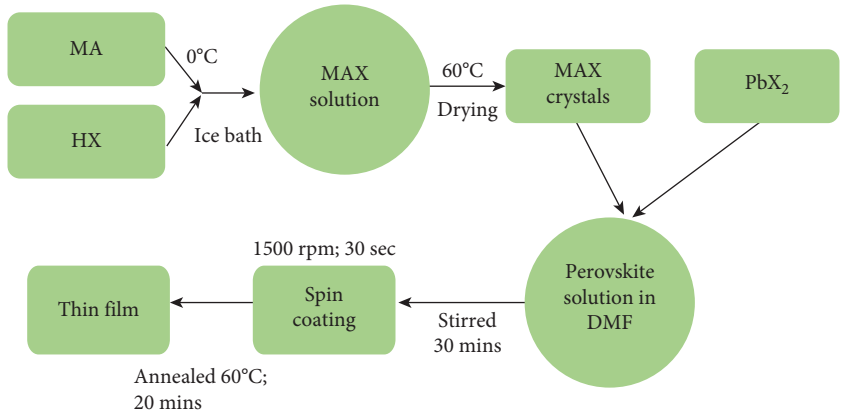

Figure 2: Flowchart of the experimental process.

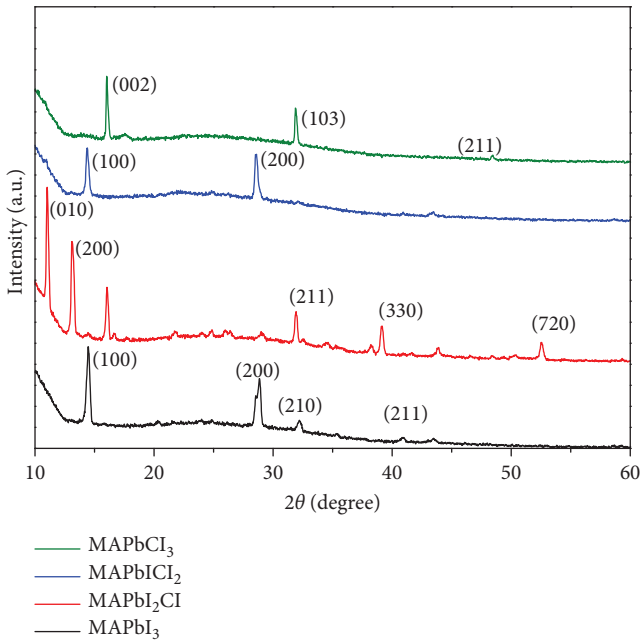

Figure 3: XRD of different synthesized perovskite materials.

Table 1: Lattice parameters and volume for synthesized materials.

Synthesized materials	Lattice parameters (Å) ($\alpha = \beta = \gamma = 90^{\circ}$)			Cell volume (Å^3)
	a	b	c	
$MAPI_3$	6.134	6.134	4.409	165.86
$MAPI_2Cl$	13.509	13.509	3.335	362.14
$MAPICl_2$	3.122	3.122	6.142	59.86
$MAPCl_3$	4.254	4.254	11.103	200.93

3.2. Morphological Structure of Synthesized Perovskite Film. Figure 5 shows the SEM image of $MAPI_3$, $MAPI_2Cl$, $MAPICl_2$, and $MAPCl_3$ perovskites. These images confirmed the crystal formation of perovskite structure and

Table 2: XRD peak positions, FWHM, average L, and δ of the prepared crystals.

Material	2θ (degree)	FWHM (degree)	Average L (nm)	δ (nm)$^{-2}$
$MAPI_3$	14.47 28.85 32.215	0.345 0.53 0.35	20.77	0.0023
$MAPI_2Cl$	11.01 13.123 31.93 39.13 52.547	0.21 0.294 0.245 0.327 0.338	30.18	0.0011
$MAPICl_2$	14.38 28.56	0.26 0.261	31.11	0.0010
$MAPCl_3$	16.029 31.89	0.171 0.22	42.23	0.0005

obtained microrod shape for $MAPI_3$ and $MAPI_2Cl$ in Figures 5(a) and 5(b), respectively. As observed in previous reports, the dendrite growth of iodine halide perovskite allows them to form in rods or wires [12, 38]. The grain structure changes drastically with decreasing iodine content and increasing chlorine in the perovskite. The microrods tend to break down with a decreasing iodine concentration in the sample. The breakdown of microrods is observed in Figure 4(b), whereas Figure 5(c) shows the growth of cuboid clusters. Finally, for $MAPCl_3$ structure (Figure 5(d)), cubic grains are observed, which satisfies previous research [39]. The average grain size of $MAPI_3$, $MAPI_2Cl$, $MAPICl_2$, and $MAPCl_3$ are 2.81 μm, 3.98 μm, 7.12 μm, and 7.2 μm, respectively. The structural deformation arises due to the change in the ionic radius of the X-site. This deformation can oppose the growth of microrods in various directions, which may cause the breakage of the rod structure into smaller cuboids. Although all the images show a poor film coverage, which can affect the optical as well as electrical properties of the materials. In order to improve the film coverage, higher DMF content can be used [40].

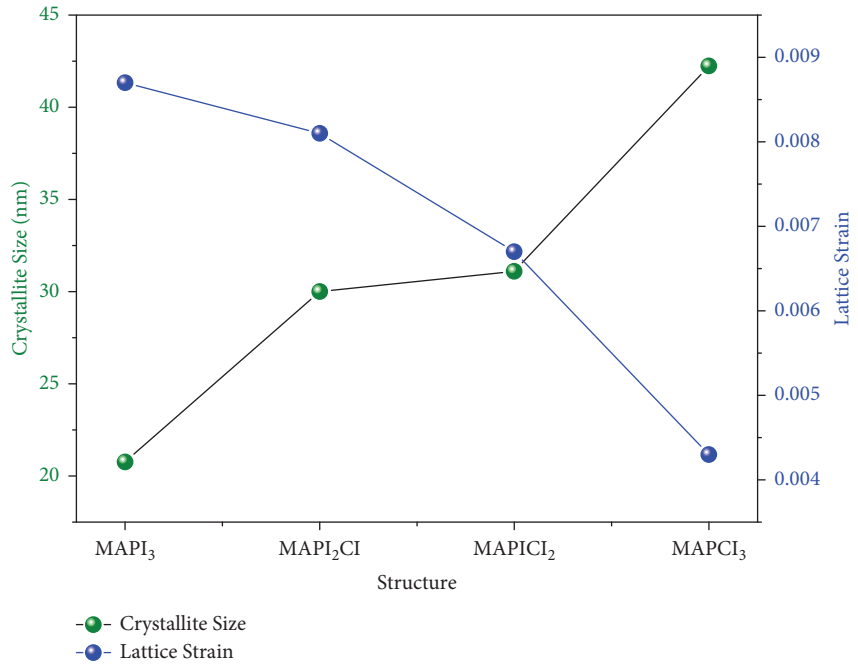

Figure 4: Crystallite size and lattice strain of the synthesized crystals.

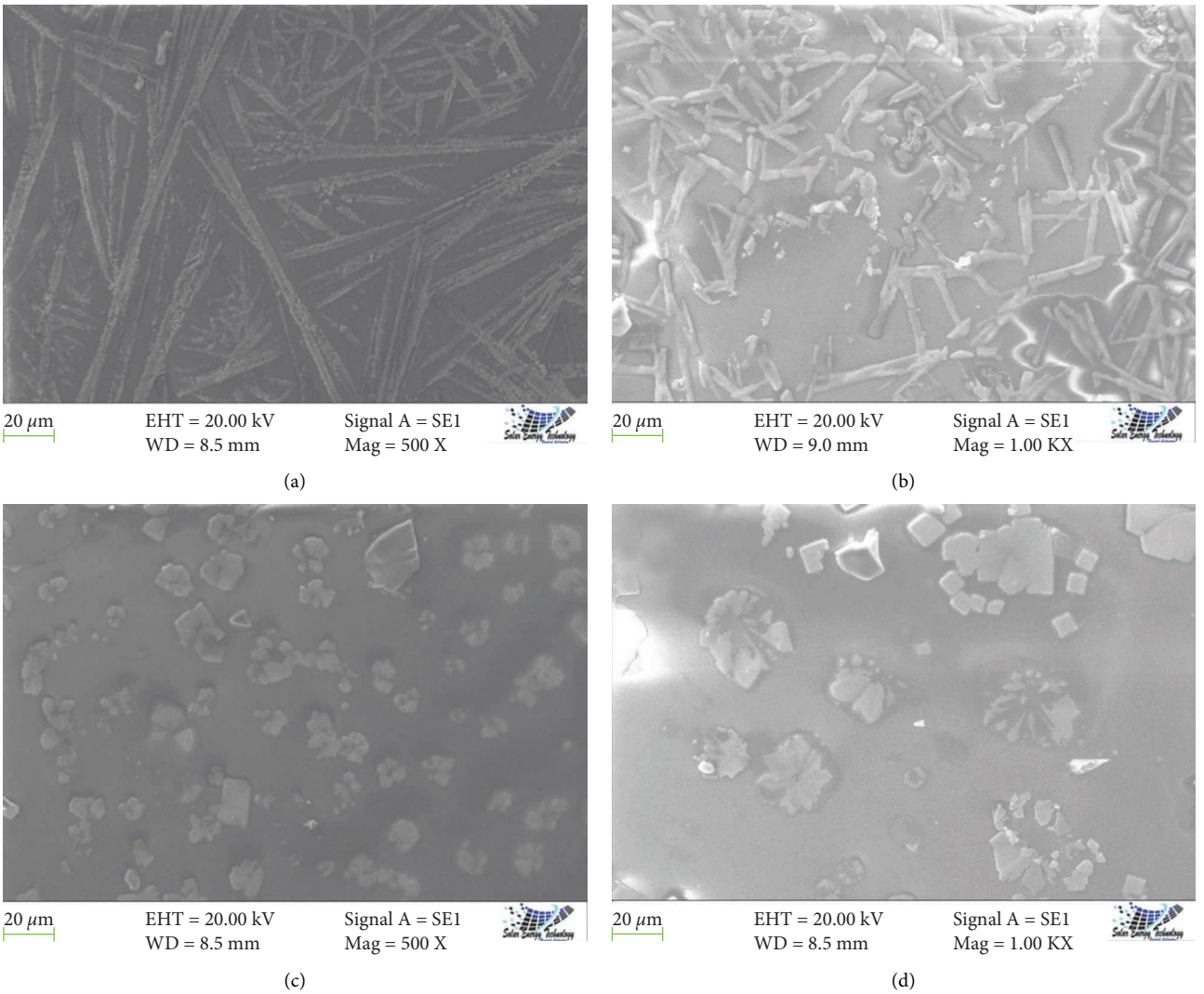

Figure 5: SEM morphological structure of (a) $MAPI_3$, (b) $MAPI_2Cl$ and (c) $MAPICl_2$, (d) $MAPCl_3$.

4. Conclusions

The $MAPI_3$, $MAPICl_2$, $MAPICl_2$, and $MAPCl_3$ perovskite thin films were successfully synthesized via the one-step spin coating method. The XRD analysis shows fine crystallinity of all the perovskite with average grain sizes of 20.77 nm, 30.01 nm, 31.11 nm, and 40.23 nm, for $MAPI_3$, $MAPICl_2$, $MAPICl_2$, and $MAPCl_3$ structures, respectively, signifying that reduction of iodine and increase of chlorine content in the halide ion site can increase crystal periodicity. All the structures showed a tetragonal phase with a variation of lattice parameters due to the lattice deformation. The grain shape also changes from rod to cube structure with the alteration of halide ions. The average grain diameter of $MAPI_3$, $MAPI_2Cl$, $MAPICl_2$, and $MAPCl_3$ are 2.81 μm, 3.98 μm, 7.12 μm, and 7.2 μm, respectively. This article deals only with the structural and morphological properties of the perovskites. However, more characterizations (i.e., optical, electrical, elemental, etc.) can be observed for these structures in future studies.

Data Availability

The data used to support the findings of this study are available from the corresponding author upon request.

Conflicts of Interest

The authors declare that there are no conflicts of interest regarding the publication of this article.

Acknowledgments

This work was supported by the Condensed Matter Physics lab, Department of Physics, Jahangirnagar University, Dhaka 1342, Bangladesh. The authors also acknowledge M. S. Bashar, Principle Scientific Officer, Bangladesh Council of Scientific and Industrial Research, for providing necessary characterization techniques. This research was funded by the National Science and Technology (NST) fellowship under the Ministry of Science and Technology, Bangladesh.

References

[1] S. Shi, Y. Li, X. Li, and H. Wang, "Advancements in all-solid-state hybrid solar cells based on organometal halide perovskites," *Materials Horizons*, vol. 2, pp. 1–28, 2015.

[2] N. G. Park, "Perovskite solar cells: an emerging photovoltaic technology," *Materials Today*, vol. 18, no. 2, pp. 65–72, 2015.

[3] C. Wang, Y. Chen, B. Zhang et al., "High-efficiency bulk heterojunction memory devices fabricated using organometallic halide perovskite:poly (N-vinylcarbazole) blend active layers," *Dalton Transactions*, vol. 45, no. 2, pp. 484–488, 2016.

[4] A. R. Pascoe, N. W. Duffy, A. D. Scully, F. Huang, and Y. B. Cheng, "Insights into planar $CH_3NH_3PbI_3$ perovskite solar cells using impedance spectroscopy," *Journal of Physical Chemistry C*, vol. 119, no. 9, pp. 4444–4453, 2015.

[5] G. Adam, M. Kaltenbrunner, E. D. Głowacki et al., "Solution processed perovskite solar cells using highly conductive PEDOT:PSS interfacial layer," *Solar Energy Materials and Solar Cells*, vol. 157, pp. 318–325, 2016.

[6] B. S. Yilbas, A. Al-Sharafi, and H. Ali, "Surfaces for self-cleaning," *Self-Cleaning Surfaces Water Droplet Mobile*, pp. 45–98, 2019.

[7] Z. Xiao, C. Bi, Y. Shao et al., "Efficient, high yield perovskite photovoltaic devices grown by interdiffusion of solution-processed precursor stacking layers," *Energy and amp;amp; Environmental Science*, vol. 7, no. 8, pp. 2619–2623, 2014.

[8] G. E. Eperon, S. D. Stranks, C. Menelaou, M. B. Johnston, L. M. Herz, and H. J. Snaith, "Formamidinium lead trihalide: a broadly tunable perovskite for efficient planar heterojunction solar cells," *Energy and amp;amp; Environmental Science*, vol. 7, no. 3, p. 982, 2014.

[9] L. Bertoluzzi, "Light induced structural changes in $CH_3NH_3PbI_3$ perovskite solar cells," *Journal of Physics Conference Series*, vol. 609, Article ID 012001, 2015.

[10] H. Kim, K. G. Lim, and T. W. Lee, "Planar heterojunction organometal halide perovskite solar cells: roles of interfacial layers," *Energy and amp;amp; Environmental Science*, vol. 9, no. 1, pp. 12–30, 2016.

[11] Q. Lin, A. Armin, R. C. R. Nagiri, P. L. Burn, and P. Meredith, "Electro-optics of perovskite solar cells," *Nature Photonics*, vol. 9, no. 2, pp. 106–112, 2015.

[12] M. T. Ahmed, S. Islam, M. S. Bashar, M. A. Hossain, and F. Ahmed, "Synthesis and characterizations of CH3NH3PbI3: ZnS," *Advances in Materials Science and Engineering*, vol. 2022, Article ID 7606339, 14 pages, 2022.

[13] H. J. Snaith, "Perovskites: the emergence of a new era for low-cost, high-efficiency solar cells," *The Journal of Physical Chemistry Letters*, vol. 4, no. 21, pp. 3623–3630, 2013.

[14] M. M. Lee, J. Teuscher, T. Miyasaka, T. N. Murakami, and H. J. Snaith, "Efficient hybrid solar cells based on meso-superstructured organometal halide perovskites," *Science*, vol. 338, no. 6107, pp. 643–647, 2012.

[15] P. Su, Y. Liu, J. Zhang et al., "Pb-based perovskite solar cells and the underlying pollution behind clean energy: dynamic leaching of toxic substances from discarded perovskite solar cells," *Journal of Physical Chemistry Letters*, vol. 11, no. 8, pp. 2812–2817, 2020.

[16] Q. Mo, C. Chen, W. Cai, S. Zhao, D. Yan, and Z. Zang, "Room temperature synthesis of stable zirconia-coated $CsPbBr_3$ nanocrystals for white light-emitting diodes and visible light communication," *Laser and Photonics Reviews*, vol. 15, no. 10, Article ID 2100278, 2021.

[17] I. Jeong-Hyeok, I. H. Jang, N. Pellet, M. Grätzel, and N. G. Park, "Growth of $CH_3NH_3PbI_3$ cuboids with controlled size for high-efficiency perovskite solar cells," *Nature Nanotechnology*, vol. 9, no. 11, pp. 927–932, 2014.

[18] W. Nei, T. Hsinhan, A. Reza et al., "High-efficiency solution-processed perovskite solar cells with millimeter-scale grains," *Science*, vol. 347, pp. 522–525, 2015.

[19] H. Zhou, Q. Chen, G. Li et al., "Interface engineering of highly efficient perovskite solar cells," *Science*, vol. 345, no. 6196, pp. 542–546, 2014.

[20] D. Y. Son, J. W. Lee, Y. J. Choi et al., "Self-formed grain boundary healing layer for highly efficient $CH_3NH_3PbI_3$ perovskite solar cells," *Nature Energy*, vol. 1, no. 7, pp. 16081–16088, 2016.

[21] B. Wang, J. Peng, X. Yang et al., "Template Assembled large-size $CsPbBr_3$ nanocomposite films toward flexible, stable, and high-performance X-ray scintillators," *Laser and Photonics Reviews*, vol. 16, no. 7, Article ID 2100736, 2022.

[22] H. Xiao, J. Fu, X. Wei et al., "Photoelectron-extractive and ambient-stable $CsPbBr_3$ @SnO_2 nanocrystals for high-performance photodetection," *Laser and Photonics Reviews*, Article ID 2200276, 2022.

[23] T. Zhou, M. Wang, Z. Zang, and L. Fang, "Stable dynamics performance and high efficiency of ABX_3-type super-alkali perovskites first obtained by introducing H_5O_2 cation," *Advanced Energy Materials*, vol. 9, no. 29, Article ID 1900664, 2019.

[24] M. Wang, H. Wang, W. Li, X. Hu, K. Sun, and Z. Zang, "Defect passivation using ultrathin PTAA layers for efficient and stable perovskite solar cells with a high fill factor and eliminated hysteresis," *Journal of Materials Chemistry*, vol. 7, no. 46, pp. 26421–26428, 2019.

[25] Best Research-Cell, *Efficiency Chart | Photovoltaic Research*, NREL, 2021, https://www.nrel.gov/pv/cell-efficiency.html.

[26] N. J. Jeon, J. H. Noh, Y. C. Kim, W. S. Yang, S. Ryu, and S. Il Seok, "Solvent engineering for high-performance inorganic-organic hybrid perovskite solar cells," *Nature Materials*, vol. 13, pp. 1–7, 2014.

[27] M. Jiang, J. Wu, F. Lan, Q. Tao, D. Gao, and G. Li, "Enhancing the performance of planar organo-lead halide perovskite solar cells by using a mixed halide source," *Journal of Materials Chemistry*, vol. 3, pp. 963–967, 2015.

[28] W. Liu and Y. Zhang, "Electrical characterization of TiO_2/$CH_3NH_3PbI_3$heterojunction solar cells," *Journal of Materials Chemistry*, vol. 2, no. 26, pp. 10244–10249, 2014.

[29] S. Colella, E. Mosconi, P. Fedeli et al., "$MAPbI_{3-x}Cl_x$ mixed halide perovskite for hybrid solar cells: the role of chloride as dopant on the transport and structural properties," *Chemistry of Materials*, vol. 25, no. 22, pp. 4613–4618, 2013.

[30] J. H. Heo and S. H. Im, "Highly reproducible, efficient hysteresis-less $CH_3NH_3PbI_{3-x}Cl_x$planar hybrid solar cells without requiring heat-treatment," *Nanoscale*, vol. 8, no. 5, pp. 2554–2560, 2016.

[31] P. Fan, D. Gu, G. X. Liang et al., "High-performance perovskite $CH_3NH_3PbI_3$ thin films for solar cells prepared by single-source physical vapour deposition," *Scientific Reports*, vol. 61, pp. 29910–29919, 2016.

[32] F. Qian, J. Gong, M. Hu et al., "p–p orbital interaction via magnesium isovalent doping enhances optoelectronic properties of halide perovskites," *Chemical Communications*, vol. 56, no. 100, pp. 15639–15642, 2020.

[33] M. Caputo, N. Cefarin, A. Radivo et al., "Electronic structure of $MAPbI_3$ and $MAPbCl_3$: importance of band alignment," *Scientific Reports*, vol. 9, pp. 15159–15211, 2019.

[34] P. Docampo, F. C. Hanusch, N. Giesbrecht, P. Angloher, A. Ivanova, and T. Bein, "Influence of the orientation of methylammonium lead iodide perovskite crystals on solar cell performance," *APL Materials*, vol. 2, no. 8, Article ID 081508, 2014.

[35] D. A. A. Leal, B. Krishnan, S. Shaji, and D. A. Avellaneda, "On the structure and physical properties of methyl ammonium lead iodide perovskite thin films by the two-step deposition method," *Materials Chemistry and Physics*, vol. 215, pp. 137–147, 2018.

[36] M. T. Ahmed, S. Islam, and F. Ahmed, "Comparative study on the crystallite size and bandgap of perovskite by diverse methods," *Advances in Condensed Matter Physics*, vol. 2022, Article ID 9535932, 7 pages, 2022.

[37] A. Goktas, F. Aslan, A. Tumbul, and S. H. Gunduz, "Tuning of structural, optical and dielectric constants by various transition metal doping in ZnO: TM (TM = Mn, Co, Fe) nanostructured thin films: a comparative study," *Ceramics International*, vol. 43, no. 1, pp. 704–713, 2017.

[38] T. B. Song, Q. Chen, H. Zhou et al., "Perovskite solar cells: film formation and properties," *Journal of Materials Chemistry*, vol. 3, no. 17, pp. 9032–9050, 2015.

[39] G. Xing, N. Mathews, S. S. Lim et al., "Facile solvothermal method to synthesize hybrid perovskite $CH_3NH_3PbX_3$ (X = I, Br, Cl) crystals," *Optical Materials Express*, vol. 7, no. 11, pp. 4156–4162, 2017.

[40] M. T. Ahmed, S. Islam, and F. Ahmed, "Optical and electrical properties of perovskite microrods," *Materialwissenschaft und Werkstofftechnik*, vol. 53, no. 7, pp. 790–797, 2022.